Research Article Vol. 9, No. 3 / March 2022 / Optica 309

OPTICA

All-optical dynamic modulation of spontaneous emission rate in hybrid optomechanical emitter-cavity systems

Feng Tian,[1,2] Hisashi Sumikura,[1,3] Eiichi Kuramochi,[1,3] Masato Takiguchi,[1,3] Masaaki Ono,[1,3] Akihiko Shinya,[1,3] and Masaya Notomi[1,2,3,*]

[1]NTT Basic Research Laboratories, NTT Corporation, 3-1 Morinosato Wakamiya, Atsugi, Kanagawa 243-0198, Japan
[2]Department of Physics, Tokyo Institute of Technology, 2-12-1-H55 Ookayama, Meguro, Tokyo 152-8550, Japan
[3]Nanophotonics Center, NTT Corporation, 3-1 Morinosato Wakamiya, Atsugi, Kanagawa 243-0198, Japan
*Corresponding author: notomi@phys.titech.ac.jp

Received 29 September 2021; revised 10 February 2022; accepted 19 February 2022; published 16 March 2022

Optomechanics is the study of the interaction between nano-objects and light fields through radiation pressure. Recent sophisticated optomechanical systems consist of strongly coupled mechanical and optical resonators and are made using semiconductor nanofabrication techniques. Although the optomechanical systems have exhibited their powerful capability of controlling photons, they are scarcely used to control the solid-state artificial atoms that emit photons. The main reason is that an efficient coupling mechanism remains unexplored. Here, we hybridize a silicon-integrated optomechanical resonator with two-level atom-like emitters to demonstrate an optomechanical cavity quantum electrodynamic (cQED) effect. With this system and the effect, we realize the dynamic modulation of the spontaneous emission rate. We choose copper dopants in silicon as the emitters for its narrow linewidth (0.3 nm) and long lifetime (∼30 ns). Our judiciously designed coupled-nanobeam optomechanical resonator achieves a strong Purcell effect and high cavity-modulation performances. The optical cavity of the optomechanical resonator is dynamically coupled to the emission line and, as a result, on-demand sharp pulses (up to 9.5-fold intensity enhancement and 3.5 ns in duration, which is one ninth of the emission lifetime) appear along the photoluminescence decay. These experimental results are exactly explained with an analytical model that combines optomechanical and cQED theories. Considering that dopants in silicon are highly competitive qubits, we believe that our optomechanical cQED technology will find important applications in the quantum era.

https://doi.org/10.1364/OPTICA.444781

1. INTRODUCTION

Mechanical systems ranging in size from the macroscale (e.g., Advanced LIGO) to the microscale (e.g., micro-electro-mechanical projectors [1]) are tools that are widely used to control optical systems. With the development of nanophotonic devices, a new field of nanoscale optomechanics has blossomed [2,3]. One of the most important aspects of this field is the study of the interaction between optical cavities and mechanical oscillators. Relevant theories have been examined [4] and many applications have been proposed [5–8]. However, the photonic devices have been coupled with solid-state atom-like emitters (for example, quantum dots (QDs) and crystal defects) through cavity quantum electrodynamic (cQED) effects [9,10], but the optomechanical systems have not been developed in this direction. We can expect that, by combining the optomechanical and cQED effects, one can dynamically modulate the optical transitions of the two-level emitters due to dynamic emitter-cavity coupling (see a pioneering proposal in Ref. [11]). This hybrid effect may find applications in photonic integrated circuits and photonic quantum technologies, such as ultralong photon memories and time-division readout of spin states.

Spontaneous emission (SE) is the process of atoms (or artificial atoms) transiting from an excited energy level to a lower energy level and emitting photons. The energy levels of the solid-state atom-like emitters can couple to the strain fields surrounding the emitters. Thus, on the one hand, the mechanical deformation modifying the strain fields are employed to tune the energy levels and in turn the photon wavelengths [12–14]. On the other hand, because of the emitter's state-dependent strain, the optical transition between the states induces strain difference (namely force) and thus can drive the mechanical resonator [15]. Besides the transition frequencies, the transition rates (namely the SE rates) can also be tuned by strains, but the tuning ranges are limited (for example, a reduction of up to 50% in the carrier lifetimes [16]). In contrast, the Purcell effect [17], a typical cQED effect, can significantly enhance the SE rates through cavity environments (one order of magnitude larger than the strain-controlled enhancements) [18].

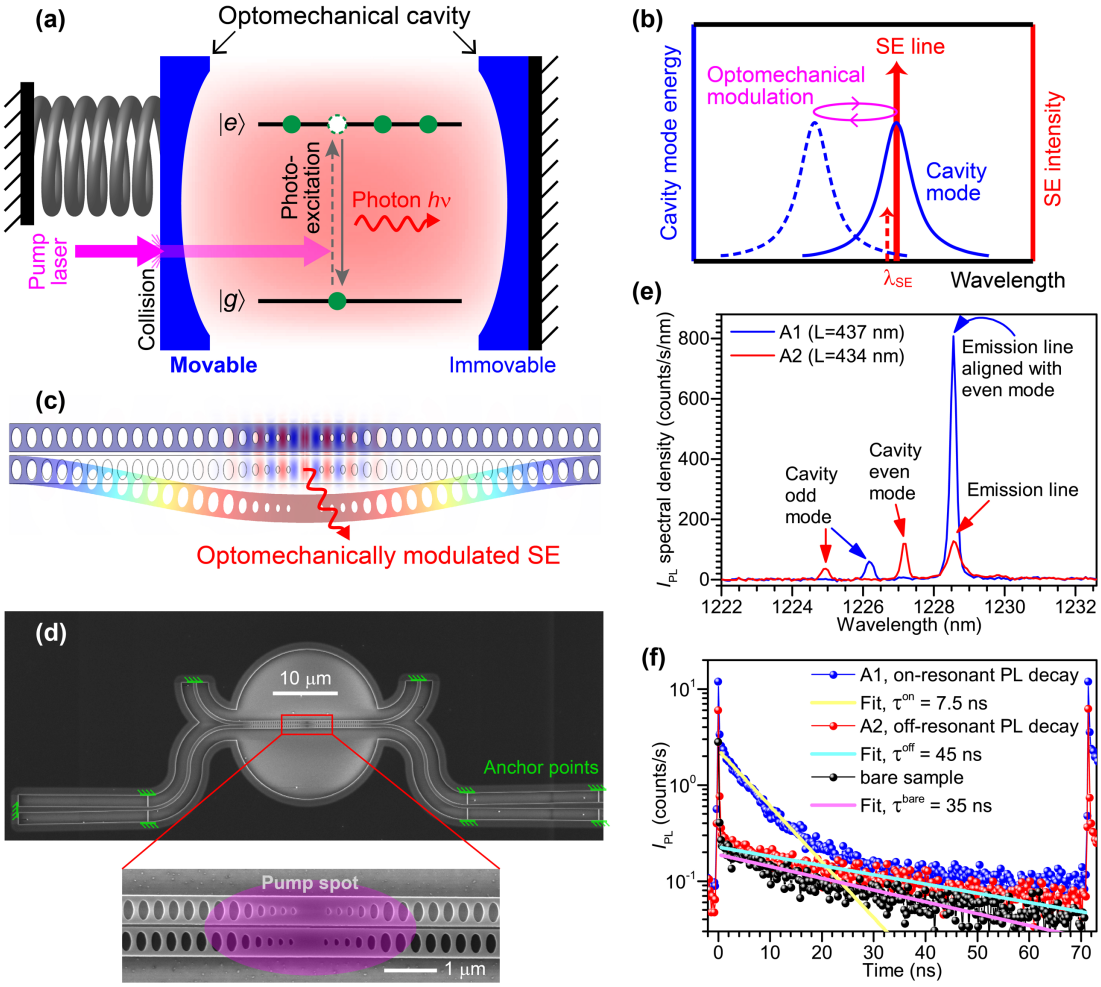

Fig. 1. Hybrid optomechanical cavity quantum electrodynamics (cQED) system. (a) The schematic diagram of the mechanized cQED system. The optical cavity is movable, so its resonance is optomechanically tunable. A pump laser is used to excite the photoluminescence (PL) of the two-level emitters embedded in the cavity and to simultaneously drive the movable part of the cavity (momentum-exchange-induced optical force). (b) The spectral illustration of the dynamics of the hybrid system. The cavity resonance is optomechanically modulated to periodically cross the spontaneous emission (SE) line, so the SE intensity is dynamically enhanced via the Purcell effect. (c) The design of the optomechanical cavity: double-coupled photonic-crystal (PhC) nanobeam cavities. Desired mechanical and optical resonance modes, simulated by finite element method (FEM), are depicted. (d) The scanning electron microscope (SEM) image of a fabricated silicon device, where Si:Cu emitters are embedded. Inset: illustration of the focused pump laser (a pulsed laser with a wavelength of 375 nm and a pulse duration of 90 ps) for the photoexcitation of the PL in the cavity region. (e) The PL spectra of two immovable devices with slightly different cavity lengths (L) (A1 with the emission line on the cavity resonance and A2 with that off the cavity resonance). (f) The time-resolved PL decay curves of the emission lines in the A1, the A2, and a bare region of the same sample, respectively. Solid curves: mono-exponential fits. Condition of the pump laser: a pulse energy of 7.3 pJ and a repetition rate of 14 MHz.

Therefore, the dynamic modulation of the Purcell effect becomes a promising way to dynamically modulate the SE rates. Recently, reshaped photoluminescence (PL) decay has been experimentally demonstrated in several cQED systems, and the underlying mechanism has proved to be the modulated Purcell effect and thus the modulated SE rates within the emission lifetimes [19–21]. These experiments were realized with different methods, such as laser-pulse-induced carrier injection [19], the Stark effect [20], and surface acoustic waves [21]. Although these methods were effective to some extent, they were unable to achieve the transient bursts of the SE rate (that is, the pulses along the PL decay) because the modulation speeds and the Purcell enhancements are insufficient. In addition, all these methods inevitably changed the energy levels of the emitters, which is undesirable for the applications requiring stable Jaynes–Cummings ladders [22].

In this study, we experimentally realize the optomechanical modulation of the Purcell effect, which is the first silicon-integrated optomechanical resonator working on a cQED. The experimental results will show a sizeable leap of the modulation performances from the previous methods. In our system, the modulated PL intensity is enhanced by about one order of magnitude, the modulation speed is almost one order of magnitude faster than the intrinsic SE rate of the emitters, and the strain effect on the emission wavelength (that is, the emitters' energy levels) is negligible.

The schematic diagram of our system is shown in Fig. 1(a), and its spectral dynamics is illustrated in Fig. 1(b). Two-level emitters are embedded in a high-quality (Q) optical cavity, enabling the Purcell effect, and the cavity resonance is modulated by mechanical oscillation via optomechanical coupling. Because the modulated cavity dynamically couples with the emitters (a dynamic Purcell

effect), the SE rate and thus the emission intensity are dynamically modulated. To achieve the emission bursts along the PL decay, the cavity mode should cross the emission line rapidly with a strong Purcell effect. Thus, three factors are crucial: the emitters with a narrow emission linewidth and a long lifetime, the optomechanical configuration with a fast-moving mechanical oscillator and a strong optomechanical coupling, and the significant Purcell factor. Here, we employ copper dopants in silicon (Si:Cu) as the two-level emitters for three reasons. First, dopants in silicon feature their sharp emission lines and long lifetimes [23,24]. Our Si:Cu ensemble shows an emission linewidth of 0.3 nm (comparable to those of single QDs in III–V semiconductors [20,21]) and a PL decay time of ∼30 ns [much longer than those of QDs (∼1 ns)]. In addition, we have observed the strong Purcell effect for our Si:Cu ensemble in a photonic crystal (PhC) cavity [25]. Second, the dopants in silicon have been considered as highly competitive qubits [22], which indicates that our study has broad implications for the development of quantum technologies. Third, silicon is a superior material for both mechanical and optical resonators, and its nanofabrication techniques are mature and low-cost.

We employ double-coupled PhC nanobeam cavities as the optomechanical configuration. The double-nanobeam cavity has strong optomechanical coupling and large displacement amplitudes [3,26,27], so the cavity resonance can be mechanically modulated in a wide spectral range. Although optomechanical crystal structures [28] exhibit gigahertz vibration frequencies, the displacement amplitude is too small (picometer scale or less) to tune the cavity resonance across the emission line. With our device, the wavelength of the cavity resonance is modulated to as wide as 6.6 nm (22 times larger than the Si:Cu emission linewidth) and crosses the emission line in 3.5 ns (one ninth of the PL decay time). Hence, we selected the most appropriate platform for realizing the dynamic optomechanical modulation of the SE rates proposed in Figs. 1(a) and 1(b).

2. PURCELL EFFECT IN IMMOVABLE CAVITY

Our optomechanical cavity system is shown in Fig. 1(c). Each optical cavity of the pair is formed by a PhC defect in the central region of the nanobeam, which is specially designed to keep a sufficiently large space for the Si:Cu emitters (see Supplement 1, Section 1 for the optical design). The devices [see Fig. 1(d)] are fabricated in two steps [25]. First, the emitters are formed in the silicon device layer of a silicon-on-insulator (SOI) wafer by Cu-ion implantation and rapid thermal annealing. Second, the nanostructures are fabricated by electron beam lithography, reactive ion etching, and hydrofluoric vapor etch release.

As a prerequisite, we verified the Purcell effect of our cavity for the Si:Cu emitters by employing the same optical design but with mechanically immovable cavities [anchors were set between the nanobeams. See Supplement 1, Fig. S4(a)]. Figure 1(e) shows the PL spectra of two immovable devices (A1 and A2) with slightly different cavity lengths. Odd and even cavity modes were identified by performing finite element method (FEM) simulations. Hereafter, we are interested in the even mode because it has a much stronger optomechanical coupling than the odd one [26,27]. Note that the even mode of the A1 device overlaps with the emission line (wavelength λ_e) at 1228.6 nm, and the emission intensity is enhanced by 6.7 times compared with that of the A2 device, in which the emission line is away from any cavity resonance. We also performed time-resolved PL decay measurements [see Fig. 1(f)]. The decay time of A1 is 7.5 ns while that of A2 is 45 ns. Figure 1(f) also shows the PL decay curve of a bare region of the same sample, whose decay time is 35 ns. The PL decay of A1 is also significantly accelerated from that of the bare sample, which is the exact evidence of the Purcell effect (see the similar verification of the Purcell effect for Si:Cu PhC slab cavities [25]). That is to say, the new optical design (that is, the double-coupled PhC nanobeam cavity) proves effective in generating a significant Purcell effect.

3. OPTOMECHANICAL CHARACTERIZATION OF MOVABLE CAVITY

Here, we use a movable-cavity device (B1), which has no anchor between the nanobeams, to investigate the optomechanical characteristics with the setup shown in Fig. 2(a). We choose the in-plane fundamental mechanical resonance mode of the longer nanobeam [see Fig. 2(a), inset], whose resonance frequency is designed to be 4.1 MHz. A pulsed ultraviolet laser (375 nm in wavelength so the photon energy is sufficiently large for the photoexcitation) is used to excite the PL and simultaneously drive the mechanical oscillation. The driving force is generated by the photons exchanging momentum with the mechanical oscillator [see Fig. 1(a) for an illustration]. In the setup of Fig. 2(a), the pulse train exerts periodic force on the nanobeam oscillator, and the optomechanical modulation is excited when the pulse repetition rate (referred to as the f_{rep}) is tuned to the mechanical resonance frequency of the nanobeam. As explained in Section 3 of Supplement 1, an f_{rep} value of around 4 MHz does not cause any heat accumulation in the emitters when the pulse energy is optimized to be 9.8 pJ/pulse. Hereafter, we employ this pulse energy for pumping. In addition, this pulse energy does not result in any thermo-optic tuning of the cavity [3,26] [see Fig. 2(b) and Supplement 1, Fig. S5(a)], so the optomechanical effect is the only mechanism by which the cavity is modulated.

Figure 2(b) shows the PL spectrum of the B1 excited device with the $f_{rep} = 4.0$ MHz. Since the f_{rep} is off-resonant from the mechanical resonance frequency (4.1 MHz), this result represents an unmodulated cavity (static wavelength $\lambda_{cav,st}$). One can see that the emission line (58.8 GHz wide) is completely detuned from the cavity mode (37.5 GHz wide) by 1.27 nm (255 GHz). Before proceeding to the SE modulation experiment, we calibrated the modulation performance of B1 with an auxiliary probe (a tunable continuous-wave laser in the 1.2 μm band). The probe laser was launched into the cavity through the waveguide, and the transmitted light was detected through the objective lens above the cavity [see Fig. 2(a)]. By setting the probe wavelength (λ_{probe}) to the $\lambda_{cav,st}$ and sweeping the f_{rep} of the pump laser, we measured the resonance of the mechanical oscillator at around 4.1 MHz [see Fig. 2(a), inset]. This peak frequency matches the designed value for the mode of interest. Note that the measured peak cannot provide us more information about the optomechanical modulation, so we did the following characterization work.

We determined whether the cavity resonance can be dynamically tuned to the emission line by using optomechanical modulation. Here, we measured the time-resolved transmitted probe signals to plot the trajectory of the modulated cavity resonance. The inset of Fig. 2(c) shows an example of the time-resolved transmitted probe signal in a single modulation period when the $f_{rep} = 4.094$ MHz and the $\lambda_{probe} = \lambda_e$. Note that the probe intensity has sharp peaks at t_1 and t_2. This indicates that the cavity resonance wavelength (λ_{cav}) passes the λ_{probe} twice in a single

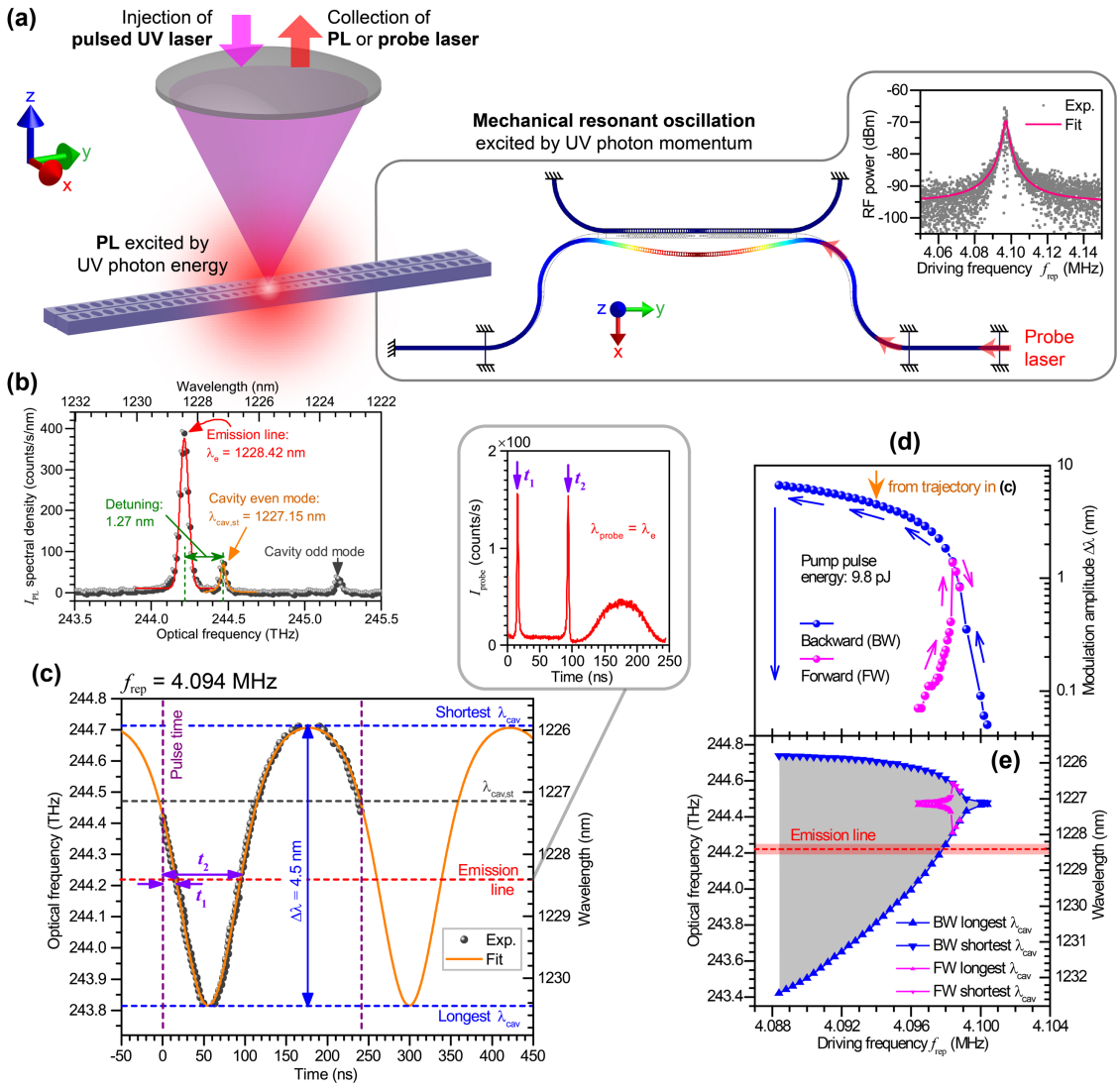

Fig. 2. Optomechanical characteristics of the device (B1) prepared for SE modulation. (a) The experimental scheme to excite both the PL and the mechanical resonant oscillation with the pulsed pump laser. Lower right inset: FEM-simulated mechanical resonance mode of interest (see Supplement 1, Fig. S2). As illustrated, a tunable continuous-wave laser (wavelength λ_{probe}) is launched into the cavity along the waveguide to probe the mechanical oscillation. Upper right inset: measured resonance spectrum of the mode (solid curve: Lorentz fit), showing a resonance frequency of ~4.1 MHz. (b) The PL spectrum of B1 excited with a pulse repetition rate (f_{rep}) of 4 MHz (off-resonant condition) and a pulse energy of 9.8 pJ/pulse, where the emission line (λ_e, Solid curve: Gaussian fit) and the unmodulated cavity's even resonance mode ($\lambda_{cav,st}$, Solid curve: Lorentzian fit) are indicated. (c) The measured and fitted trajectory of the optomechanically modulated cavity resonance (λ_{cav}) at the $f_{rep} = 4.094$ MHz, indicating modulation amplitude ($\Delta\lambda$) and boundaries (the longest and shortest λ_{cav}). Inset: time-resolved intensity of the probe transmitted through the cavity, from which the time points (t_1 and t_2) of the λ_{cav} crossing the λ_{probe} (note that we set the $\lambda_{probe} = \lambda_e$ for this plot) are determined. The λ_{cav} trajectory was plotted as a series of t_1 and t_2 by sweeping the λ_{probe}. (d) The $\Delta\lambda$ as a function of the f_{rep}, which was acquired by plotting the λ_{cav} trajectories for varying f_{rep}. The curve of the backward sweep does not coincide with that of the forward sweep, which is manifested as a softening Duffing nonlinearity of the mechanical oscillator. (e) The modulation range (grey area) of the λ_{cav} as a function of the f_{rep}. The red belt represents the emission line with its own width.

oscillation period. That is to say, at t_1 and t_2 the λ_{cav} shifts to the wavelength indicated by the probe laser (λ_{probe}). We repeated this measurement for various λ_{probe} wavelengths (see Supplement 1, Fig. S9) and determined t_1 and t_2 for the observed probe peaks. Figure 2(c) shows the summarized t_1 and t_2 for the swept λ_{probe}. We can recognize the dot curve as the time-dependent λ_{cav}, a sinusoidal-like function but with some deviations.

The nanobeam resonant oscillation can be seen as a simple harmonic motion, but the trajectory of the modulated cavity resonance is not strictly sinusoidal. This is reasonable because the λ_{cav} and the mechanical displacement of the oscillator do not strictly follow a linear relation [26,27]. In fact, the derivative of the cavity resonance with respect to the displacement (optomechanical coupling coefficient [3], $g_{OM}/2\pi$) depends on the slot gap between the nanobeams (see Supplement 1, Fig. S10 for the simulated $g_{OM}/2\pi$ as a function of the slot gap). When we included the simulated $g_{OM}/2\pi$ in the simple harmonic motion model [see Supplement 1, Eqs. (S1) and (S2)], the model fitted the measured trajectory well, as shown in Fig. 2(c). Hence, we quantitatively confirm the trajectory of the λ_{cav} modulated by the targeted mechanical resonant oscillation. In addition, the emission line is located within the modulation range, and the t_1 value (~16 ns) is shorter than the PL

decay time. This means that the modulation of the λ_{cav} is wide and fast enough for the SE modulation experiment. Thus, this device (B1) was also used in the subsequent experiment.

From the trajectory curve in Fig. 2(c), the λ_{cav} modulation amplitude ($\Delta\lambda$) for the $f_{rep} = 4.094$ MHz is found to be 4.5 nm. In Fig. 2(d), we plot the $\Delta\lambda$ determined from a series of measurements with varying f_{rep}. Here, $\Delta\lambda$ shows peculiar hysteresis as a function of the f_{rep}. This hysteresis reminds us of the behavior of the displacement amplitude of a nonlinear Duffing oscillator [29,30]. In fact, the $\Delta\lambda$ is monotonically related to the displacement amplitude of our oscillator because $g_{OM}/2\pi$ is always positive (from about 10 to 50 GHz/nm in Supplement 1, Fig. S10). That is to say, the $\Delta\lambda$ hysteresis must correspond to a displacement-amplitude hysteresis. Thus, it is demonstrated that the nanobeam oscillator used for the hybrid system is a Duffing oscillator. As shown in Fig. 2(d), $\Delta\lambda$ becomes large when the f_{rep} is swept backward. In fact, the trajectory in Fig. 2(c) ($f_{rep} = 4.094$ MHz) was obtained under this condition [see the data point indicated by the orange arrow in Fig. 2(d)]. Figure 2(e) shows the modulation boundaries of the λ_{cav} (the longest and shortest λ_{cav}) as a function of the f_{rep}. This plot indicates that the λ_e falls into the modulation range when the f_{rep} is from 4.098 to 4.088 MHz along the backward sweep.

4. MODULATED SE IN HYBRID OPTOMECHANICAL cQED SYSTEM

Next, we removed the probe laser and measured the temporal response of the modulated SE. Figure 3(a) shows the results of the PL decay measurements for device B1 driven at a backward-swept f_{rep}. When the $f_{rep} = 4.099$ MHz, at which the modulation amplitude is so small that the λ_{cav} cannot reach λ_e, the PL intensity decays exponentially, similar to the off-resonant PL decay of the immovable cavity shown in Fig. 1(f). However, as the f_{rep} is varied from 4.0977 to 4.088 MHz, the exponential decay is interrupted by sudden intense peaks at certain elapsed times. For example, when the $f_{rep} = 4.094$ MHz, there are two peaks along the decay curve, and their elapsed time after the pulse excitation (18.7 and 100 ns) are very close to t_1 and t_2 at $\lambda_{cav} = \lambda_e$ in Fig. 2(c), which strongly suggests that these peaks originate from the dynamic coupling of the cavity resonance to the emission line.

We examined these unusual PL decay curves in relation to the optomechanical dynamics characterized in Fig. 2. First, for the $f_{rep} < 4.0977$ MHz, there are always two peaks in Fig. 3(a), meaning that the λ_{cav} coincides with the λ_e twice in a single modulation period for the $f_{rep} < 4.0977$ MHz in Fig. 2(e). Second, the interval between the two peaks becomes larger as the f_{rep} decreases [see Fig. 4(b) for clarity]. These results are consistent with Fig. 2(e), where the modulation amplitude increases as the f_{rep} decreases. It can be understood from the λ_{cav} trajectory in Fig. 2(c) that a larger $\Delta\lambda$ induces a longer $|t_2 - t_1|$ at $\lambda_{cav} = \lambda_e$. Therefore, the dynamic PL intensity enhancements in Fig. 3(a) are doubtless caused by the optomechanically modulated cavity resonance. This conclusion also tells us that in our system the strain effect on the PL intensity is negligible because the strain effect has nothing to do with the cavity resonance. In addition to the PL intensity, we also verified a negligible strain effect on the emission wavelength with another experiment [see Supplement 1, Fig. S12]. Thus, we demonstrate a previously undescribed strain-free system.

It is worth noting that the peak duration at t_1 [the temporal full-width at half-maximum (FWHM) of the peaks in Fig. 3(a), summarized in Fig. 3(b)] becomes shorter as the f_{rep} decreases. This tendency can be understood by looking at the λ_{cav} trajectory in Fig. 2(c). The peak duration is determined by how fast the λ_{cav} crosses the λ_e, namely $d\lambda_{cav}(t)/dt$ [the slope of the curve in Fig. 2(c)] at $\lambda_{cav} = \lambda_e$. For smaller modulation amplitudes [higher f_{rep} in Fig. 2(e)], the λ_e is closer to the minimum of the quasi-sinusoidal λ_{cav} curve where $d\lambda_{cav}(t)/dt$ is zero, and hence, the peak lasts longer. Conversely, when the f_{rep} is lowered, the modulation range largely increases, so the λ_e becomes closer to the midpoint of the sinusoidal-like curve, where the trajectory is nearly linear and $d\lambda_{cav}(t)/dt$ is maximum. Hence, the peak duration becomes the shortest, 3.5 ns [see Fig. 3(b)], which is much shorter than the intrinsic PL decay time of our emitters (~30 ns). This is an especially interesting feature of the dynamic control of the SE by which we can change the SE properties much faster than the intrinsic radiative recombination rate.

So far, we have confirmed that the peaks are caused by the dynamic coupling of the cavity resonance to the emission line, but we have not identified the underlying mechanisms. They could be the Purcell effect (the SE rate enhancement) and/or the cavity-mode-enhanced light extraction efficiency (LEE) [31]. The theoretical Purcell factor of device B1 is approximately the same as those of A1 and A2 (see Supplement 1, Table S1), for which we have experimentally verified the Purcell effect [see Figs. 1(f)]. Thus, it is reasonable to believe that B1 would exhibit accelerated PL decay like that in A1 in Fig. 1(f) if we were able to statically tune the λ_{cav} to the λ_e. To find support for this speculation, we examined Fig. 3(a) carefully to distinguish the Purcell effect and the LEE enhancement. Figure 3(c) is a magnified plot of Fig. 3(a) indicating that the instantaneous PL intensities between t_1 and t_2 for the f_{rep} from 4.088 to 4.094 MHz are obviously smaller than that for the $f_{rep} = 4.099$ MHz, where there is no cavity-coupling-induced enhancement. This reduction is consistent only with the Purcell effect because the Purcell-enhanced radiative recombination rate should result in a rapid reduction in the exciton population after the first PL peak at t_1. In contrast, a LEE enhancement does not alter the dynamics of the exciton population. Thus, the PL intensity after the first peak should not differ from that of the $f_{rep} = 4.099$ MHz. Therefore, we confirm that the measured dynamic PL intensity enhancements [see an enhancement ratio of 9.5:1 evident in Fig. 3(a)] involve the Purcell effect. In the next step, we will prove that the Purcell effect plays a dominant role in these enhancements.

To investigate the dynamic Purcell effect quantitatively, we developed an analytical model for our hybrid optomechanical cQED system. The model provides analytical solutions for the optomechanically modulated SE process (see a full description of the model in Supplement 1, Section 5). With this model, the measured PL decay curves are fitted well [see Fig. 4(a)]. The dynamics of the corresponding exciton populations are also shown (dashed orange curves). It is clear that the exciton population decreases much faster when the PL peaks appear, which can only be explained by the Purcell-enhanced radiative recombination rate. From these fits, we obtained the on- and off-resonant radiative recombination rates (referred to as Γ_R^{on} and Γ_R^{off}, respectively), which are summarized in Supplement 1, Table S4 (mean values are $\bar{\Gamma}_R^{on} = 0.232\ ns^{-1}$ and $\bar{\Gamma}_R^{off} = 0.0135\ ns^{-1}$). From these values, we derived the non-radiative recombination rate [$\Gamma_{NR} = \Gamma_{PL}^{off} - \bar{\Gamma}_R^{off} = 0.0187\ ns^{-1}$, see Γ_{PL}^{off} in Fig. 4(a)] and the radiative recombination rate of a reference bare waveguide

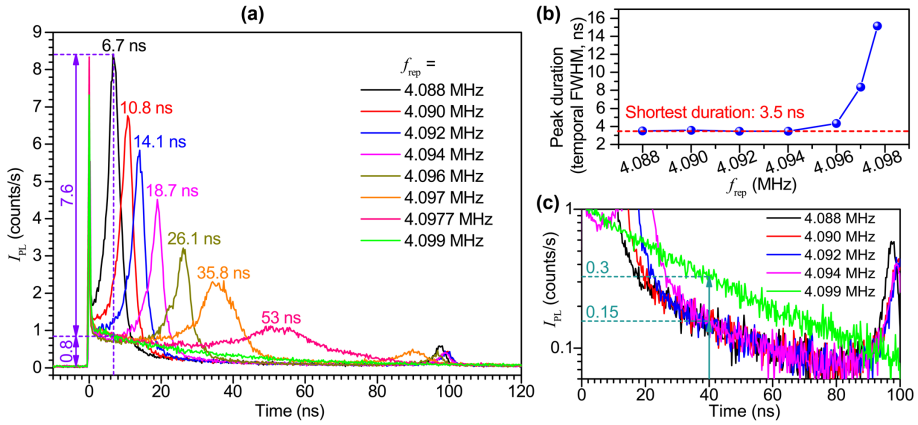

Fig. 3. Optomechanically modulated PL decay curves of B1 at varying f_{rep} (backward sweep). (a) The transient enhancements in PL intensity (I_{PL}) when the λ_{cav} crosses the λ_e, indicating the time point t_1. The measurement of each of these curves took 360 s (integration time of the superconducting single-photon detector). The curve of the $f_{rep} = 4.099$ MHz complies with a conventional PL decay because the λ_{cav} has never coupled to the λ_e, while that of the $f_{rep} = 4.088$ MHz exhibits the highest peak at 6.7 ns. By comparing the intensities (7.6 versus 0.8 counts/s), we found that the enhancement factor is 9.5. (b) The duration (temporal full-width at half-maximum) of the PL intensity peak at t_1 as a function of the f_{rep}. The duration converges to a minimum of 3.5 ns with the decrease of the f_{rep}. (c) The magnified segments of the PL decay curves between t_1 and t_2. After the λ_{cav} crosses the λ_e at t_1, the intensities for frequencies from 4.088 to 4.094 MHz are about half of that for 4.099 MHz (for example, the indicated intensities at 40 ns).

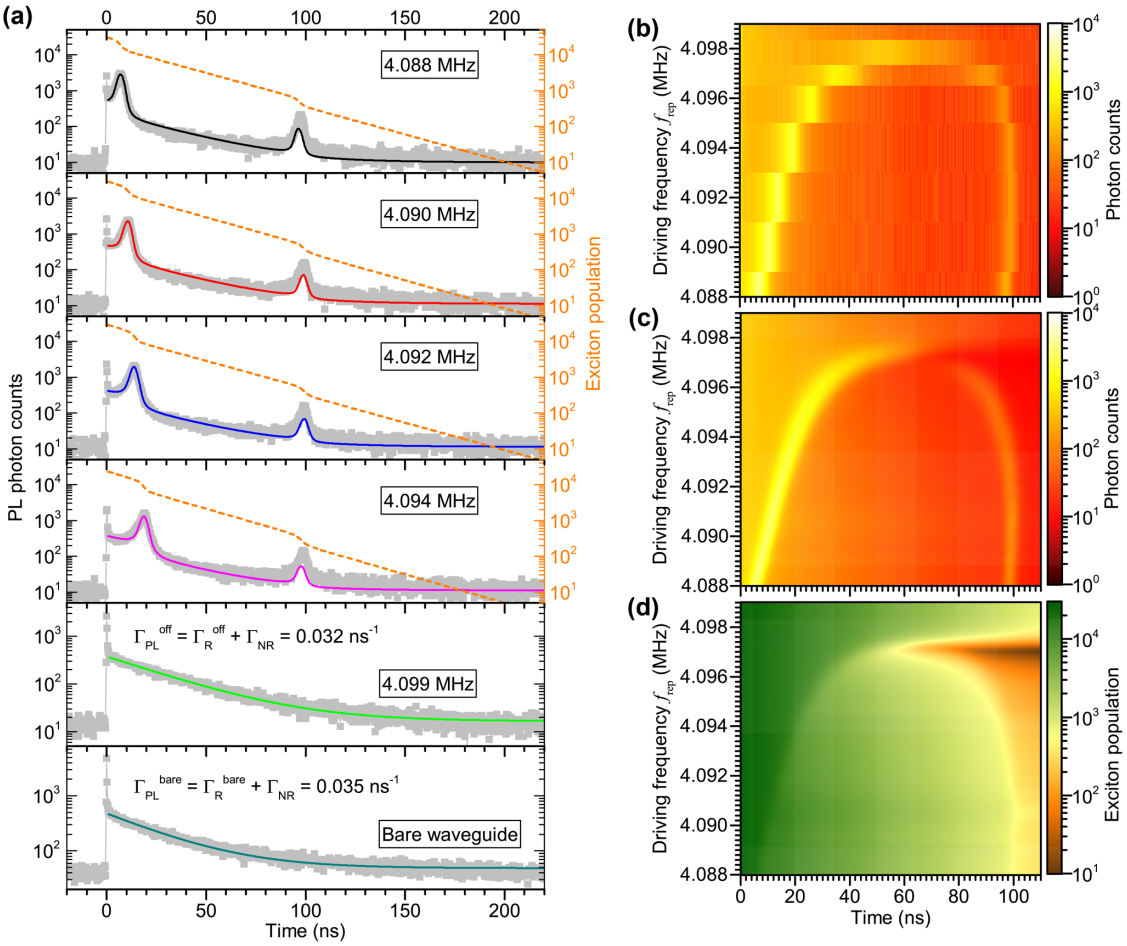

Fig. 4. Analytical model of the dynamics of the PL decay and exciton population in our hybrid optomechanical cQED system. (a) Fits (solid curves) to the measured PL decay curves [gray dots, same as those shown in Fig. 3(a)] with the analytical model. The corresponding dynamics of the exciton population (dashed orange curves) were also calculated. The off-resonant PL decay at the $f_{rep} = 4.099$ MHz and the PL decay of a neighboring reference bare waveguide ($f_{rep} = 4.099$ MHz as well) are used to deduce the experimental Purcell factor. They are fitted by a mono-exponential function (solid curves), and the corresponding PL decay rates, consisting of radiative (R) and non-radiative (NR) recombination rates, are indicated, respectively. (b) The color map of the measured PL decay [same as those shown in Fig. 3(a)] as a function of the f_{rep} for comparison. (c)–(d) The color maps of (c) the calculated PL decay and (d) the exciton population as functions of the f_{rep} (see Supplementary 1, Tables S3 and S4 for the calculation parameters).

$[\Gamma_R^{\text{bare}} = \Gamma_{\text{PL}}^{\text{bare}} - \Gamma_{\text{NR}} = 0.0167\ \text{ns}^{-1}$. See $\Gamma_{\text{PL}}^{\text{bare}}$ in Fig. 4(a)]. As a result, we determined the experimental Purcell factor ($F_P = \bar{\Gamma}_R^{\text{on}} / \Gamma_R^{\text{bare}}$) to be 13.9 for the present optomechanical cQED system. In addition, we also obtained a LEE enhancement ratio of ∼1.2 (see Supplement 1, Table S4), which was much smaller than the total enhancement ratio of 9.5 [see Fig. 3(a)]. Therefore, we conclude that the Purcell effect plays a dominant role in the measured enhancements in Fig. 3(a).

Finally, we visualized the PL decay and the exciton population as functions of the f_{rep} by using the same analytical model [see Figs. 4(c) and 4(d)], and Fig. 4(b) shows the measured data for comparison]. In addition, these two plots clearly show that the appearance of the PL peaks is accompanied by a sudden reduction in the exciton population [see Fig. 4(d)]. They also demonstrate that the timing of the Purcell enhancement (t_1 and t_2) can be tuned by changing the f_{rep} attributed to the nonlinearity of the mechanical oscillator. This interesting feature means that we can shift t_1 to 0. We have indeed achieved this condition with another device having a smaller initial separation between the λ_{cav} and the λ_e and observed a very fast monotonic PL decay, 0.299 ns^{-1} (see Supplement 1, Fig. S14).

5. DISCUSSION

The results indicate the superior performances of this first silicon-integrated optomechanical cQED system, in which a novel optomechanical cQED effect is developed. The system consists of three entities: (i) mechanical oscillators, (ii) optical cavities, and (iii) solid-state two-level emitters. Although the couplings between (i)–(ii) [2–4] or (ii)–(iii) [9,10] have been studied, the coupling among (i)–(ii)–(iii) has not been experimentally demonstrated before. Our system enables the coupling of (i)–(iii) via (ii) and provides a new mechanism to modulate the optical transitions of the solid-state quantum systems.

One possible application of this system is the synchronization of single photon pulses in integrated quantum photonic circuits because the bursts of the SE rate can be delayed at will by tuning the mechanical oscillation frequency. Although the system here is demonstrated with the Si:Cu ensemble, single dopants in silicon have been reported [32] and can be straightforwardly integrated into this system. However, note a disadvantage of the current system: because the cavity mode with a spectral width dynamically crosses the emission line, the emitted photon gets a time-dependent phase, which can make the photons distinguishable and thus limits the system for applications in single-photon sources. This problem can be solved by modulating the spatial distribution of the cavity mode rather than the mode wavelength, for example, the dark mode of the central cavity in a triple-cavity system [11]. Our system can also be improved with a triple-nanobeam optomechanical configuration [33], whose dark mode distribution is optomechanically tunable. Another possible application of our hybrid system is the time-division readout of spin states. Static cQED is usually used for the readout of one spin state [22]. To read out the other spin state, a population inversion and the second readout must be arranged in the readout sequence [34]. Our dynamic cQED system can sweep the cavity resonance widely and in turn couples the cavity to the optical transitions of the two spin states at different times, so the two states can be read out through the photon pulses distributed at the different time points, which we named time-division readout. This system may also find an application in photonic memory. Conventionally, a photon signal can only be stored in a very short time even in an ultrahigh-Q cavity (one nanosecond [35]). In contrast, the excited states of the dopants in silicon are ultralong lived (almost one millisecond [23]). One can think of storing the optical signal into the excited states via photoexcitation and reading it out by triggering the optomechanical oscillation and in turn the emission pulses.

Although the results presented here are superior, they are not the limits of this kind of hybrid optomechanical cQED systems. For example, $g_{\text{OM}}/2\pi$ can be optimized to a value of 200 GHz/nm (the current value is ∼30 GHz/nm), and the movement speed of the nanobeam can be doubled by increasing the driving force and reducing the effective mass. As a result, the pulse duration will be one order of magnitude shorter than the current value of 3.5 ns. On the emitter-cavity side, a much higher Purcell factor [18] or a strong coupling (for example, Rabi oscillations [9]) can be expected in such an optomechanical cQED system. Conclusively, the hybrid optomechanical cQED system demonstrated here is highly effective in dynamically modulating the optical transitions of solid-state quantum emitters and will find applications in photonic integrated circuits and photonic quantum technologies.

Funding. Japan Society for the Promotion of Science (15H05735).

Acknowledgment. M. N. conceived and supervised this project. F. T. conceived the experiments and designed the device. H. S. prepared the Cu-doped SOI wafers. E. K., M. O., and F. T. fabricated the device. F. T., H. S., and M. T. performed the measurements, and F. T. analyzed the results. A. S. supported the optical design and measurements. F. T. and M. N. wrote the manuscript. The authors thank S. Sergent and W. J. Munro for the valuable discussions, K. Nozaki and G. Zhang for help with the measurements, and O. Moriwaki for help with the device fabrication. The authors also acknowledge M. L. W. Thewalt for the valuable discussions.

Disclosures. The authors declare no conflicts of interest.

Data availability. Data underlying the results presented in this paper are not publicly available at this time but may be obtained from the authors upon reasonable request.

Supplemental document. See Supplement 1 for supporting content.

REFERENCES

1. P. F. Van Kessel, L. J. Hornbeck, R. E. Meier, and M. R. Douglass, "A MEMS-based projection display," Proc. IEEE **86**, 1687–1704 (1998).
2. M. Notomi, H. Taniyama, S. Mitsugi, and E. Kuramochi, "Optomechanical wavelength and energy conversion in high-Q double-layer cavities of photonic crystal slabs," Phys. Rev. Lett. **97**, 2–5 (2006).
3. M. Eichenfield, R. Camacho, J. Chan, K. J. Vahala, and O. Painter, "A picogram- and nanometre-scale photonic-crystal optomechanical cavity," Nature **459**, 550–555 (2009).
4. M. Aspelmeyer, T. J. Kippenberg, and F. Marquardt, "Cavity optomechanics," Rev. Mod. Phys. **86**, 1391–1452 (2014).
5. A. G. Krause, M. Winger, T. D. Blasius, Q. Lin, and O. Painter, "A high-resolution microchip optomechanical accelerometer," Nat. Photonics **6**, 768–772 (2012).
6. H. Li, Y. Chen, J. Noh, S. Tadesse, and M. Li, "Multichannel cavity optomechanics for all-optical amplification of radio frequency signals," Nat. Commun. **3**, 1091 (2012).
7. M. Wu, N. L.-Y. Wu, T. Firdous, F. F. Sani, J. E. Losby, M. R. Freeman, and P. E. Barclay, "Nanocavity optomechanical torque magnetometry and radiofrequency susceptometry," Nat. Nanotechnol. **12**, 127–131 (2017).
8. L. Midolo, A. Schliesser, and A. Fiore, "Nano-opto-electro-mechanical systems," Nat. Nanotechnol. **13**, 11–18 (2018).
9. T. Yoshie, A. Scherer, J. Hendrickson, G. Khitrova, H. M. Gibbs, G. Rupper, C. Ell, O. B. Shchekin, and D. G. Deppe, "Vacuum Rabi splitting with a single quantum dot in a photonic crystal nanocavity," Nature **432**, 200–203 (2004).

10. D. Englund, D. Fattal, E. Waks, G. Solomon, B. Zhang, T. Nakaoka, Y. Arakawa, Y. Yamamoto, and J. Vučković, "Controlling the spontaneous emission rate of single quantum dots in a two-dimensional photonic crystal," Phys. Rev. Lett. **95**, 013904 (2005).
11. M. Cotrufo, A. Fiore, and E. Verhagen, "Coherent atom-phonon interaction through mode field coupling in hybrid optomechanical systems," Phys. Rev. Lett. **118**, 133603 (2017).
12. Y.-I. Sohn, S. Meesala, B. Pingault, H. A. Atikian, J. Holzgrafe, M. Gundogan, C. Stavrakas, M. J. Stanley, A. Sipahigil, J. Choi, M. Zhang, J. L. Pacheco, J. Abraham, E. Bielejec, M. D. Lukin, M. Atature, and M. Loncar, "Controlling the coherence of a diamond spin qubit through its strain environment," Nat. Commun. **9**, 2012 (2018).
13. A. W. Elshaari, E. Büyüközer, I. E. Zadeh, T. Lettner, P. Zhao, E. Schöll, S. Gyger, M. E. Reimer, D. Dalacu, P. J. Poole, K. D. Jöns, and V. Zwiller, "Strain-tunable quantum integrated photonics," Nano Lett. **18**, 7969–7976 (2018).
14. M. Weiß, D. Wigger, M. Nägele, K. Müller, J. J. Finley, T. Kuhn, P. Machnikowski, and H. J. Krenner, "Optomechanical wave mixing by a single quantum dot," Optica **8**, 291–300 (2021).
15. J. Kettler, N. Vaish, L. M. de Lépinay, B. Besga, P.-L. de Assis, O. Bourgeois, A. Auffèves, M. Richard, J. Claudon, J.-M. Gérard, B. Pigeau, O. Arcizet, P. Verlot, and J.-P. Poizat, "Inducing micromechanical motion by optical excitation of a single quantum dot," Nat. Nanotechnol. **16**, 283–287 (2021).
16. C. Du, X. Huang, C. Jiang, X. Pu, Z. Zhao, L. Jing, W. Hu, and Z. L. Wang, "Tuning carrier lifetime in InGaN/GaN LEDs via strain compensation for high-speed visible light communication," Sci. Rep. **6**, 37132 (2016).
17. E. M. Purcell, "Spontaneous emission probabilities at radio frequencies," Phys. Rev. **69**, 681 (1946).
18. F. Liu, A. J. Brash, J. O'Hara, L. M. P. P. Martins, C. L. Phillips, R. J. Coles, B. Royall, E. Clarke, C. Bentham, N. Prtljaga, I. E. Itskevich, L. R. Wilson, M. S. Skolnick, and A. M. Fox, "High Purcell factor generation of indistinguishable on-chip single photons," Nat. Nanotechnol. **13**, 835–840 (2018).
19. C.-Y. Jin, R. Johne, M. Y. Swinkels, T. B. Hoang, L. Midolo, P. J. van Veldhoven, and A. Fiore, "Ultrafast non-local control of spontaneous emission," Nat. Nanotechnol. **9**, 886–890 (2014).
20. F. Pagliano, Y. Cho, T. Xia, F. van Otten, R. Johne, and A. Fiore, "Dynamically controlling the emission of single excitons in photonic crystal cavities," Nat. Commun. **5**, 5786 (2014).
21. M. Weiß, S. Kapfinger, T. Reichert, J. J. Finley, A. Wixforth, M. Kaniber, and H. J. Krenner, "Surface acoustic wave regulated single photon emission from a coupled quantum dot-nanocavity system," Appl. Phys. Lett. **109**, 33105 (2016).
22. K. J. Morse, R. J. S. Abraham, A. DeAbreu, C. Bowness, T. S. Richards, H. Riemann, N. V. Abrosimov, P. Becker, H.-J. Pohl, M. L. W. Thewalt, and S. Simmons, "A photonic platform for donor spin qubits in silicon," Sci. Adv. **3**, e1700930 (2017).
23. S. P. Watkins, U. O. Ziemelis, M. L. W. Thewalt, and R. R. Parsons, "Long lifetime photoluminescence from a deep centre in copper-doped silicon," Solid State Commun. **43**, 687–690 (1982).
24. M. Steger, A. Yang, N. Stavrias, M. L. W. Thewalt, H. Riemann, N. V. Abrosimov, M. F. Churbanov, A. V. Gusev, A. D. Bulanov, I. D. Kovalev, A. K. Kaliteevskii, O. N. Godisov, P. Becker, and H.-J. Pohl, "Reduction of the linewidths of deep luminescence centers in 28Si reveals fingerprints of the isotope constituents," Phys. Rev. Lett. **100**, 177402 (2008).
25. H. Sumikura, E. Kuramochi, H. Taniyama, and M. Notomi, "Ultrafast spontaneous emission of copper-doped silicon enhanced by an optical nanocavity," Sci. Rep. **4**, 5040 (2014).
26. P. B. Deotare, I. Bulu, I. W. Frank, Q. Quan, Y. Zhang, R. Ilic, and M. Loncar, "All optical reconfiguration of optomechanical filters," Nat. Commun. **3**, 846 (2012).
27. F. Tian, G. Zhou, Y. Du, F. S. Chau, J. Deng, X. Tang, and R. Akkipeddi, "Energy-efficient utilization of bipolar optical forces in nano-optomechanical cavities," Opt. Express **21**, 18398–18407 (2013).
28. M. Eichenfield, J. Chan, R. M. Camacho, K. J. Vahala, and O. Painter, "Optomechanical crystals," Nature **462**, 78–82 (2009).
29. M. Li, W. H. P. Pernice, C. Xiong, T. Baehr-Jones, M. Hochberg, and H. X. Tang, "Harnessing optical forces in integrated photonic circuits," Nature **456**, 480–484 (2008).
30. I. Mahboob, N. Perrissin, K. Nishiguchi, D. Hatanaka, Y. Okazaki, A. Fujiwara, and H. Yamaguchi, "Dispersive and dissipative coupling in a micromechanical resonator embedded with a nanomechanical resonator," Nano Lett. **15**, 2312–2317 (2015).
31. A. Enderlin, Y. Ota, R. Ohta, N. Kumagai, S. Ishida, S. Iwamoto, and Y. Arakawa, "High guided mode–cavity mode coupling for an efficient extraction of spontaneous emission of a single quantum dot embedded in a photonic crystal nanobeam cavity," Phys. Rev. B **86**, 75314 (2012).
32. W. Redjem, A. Durand, T. Herzig, A. Benali, S. Pezzagna, J. Meijer, A. Y. Kuznetsov, H. S. Nguyen, S. Cueff, J.-M. Gérard, I. Robert-Philip, B. Gil, D. Caliste, P. Pochet, M. Abbarchi, V. Jacques, A. Dréau, and G. Cassabois, "Single artificial atoms in silicon emitting at telecom wavelengths," Nat. Electron. **3**, 738–743 (2020).
33. X. Chew, G. Zhou, F. S. Chau, and J. Deng, "Nanomechanically tunable photonic crystal resonators utilizing triple-beam coupled nanocavities," IEEE Photon. Technol. Lett. **23**, 1310–1312 (2011).
34. J. M. Kindem, A. Ruskuc, J. G. Bartholomew, J. Rochman, Y. Q. Huan, and A. Faraon, "Control and single-shot readout of an ion embedded in a nanophotonic cavity," Nature **580**, 201–204 (2020).
35. T. Tanabe, M. Notomi, E. Kuramochi, A. Shinya, and H. Taniyama, "Trapping and delaying photons for one nanosecond in an ultrasmall high-Q photonic-crystal nanocavity," Nat. Photonics **1**, 49–52 (2007).